Long Wavelength (15 and 23 µm) GaAs/AlGaAs Quantum Cascade Lasers

J. Ulrich, J. Kreuter, W. Schrenk, G. Strasser, K. Unterrainer

Quantum cascade lasers based on GaAs/AlGaAs chirped superlattice active regions have been achieved at wavelengths of 15 (sample A) and 23 µm (sample B). In pulsed mode they operate up to temperatures of 220 K and 100 K, respectively. Sample A employs a standard waveguide with n+-doped cladding, sample B was made with a metallic surface plasmon waveguide. The threshold current densities at cryogenic temperatures of 2.2 kA/cm^2 (A) and 10.2 kA/cm^2 (B) reflect the differences in intersubband lifetimes and waveguide losses close to the reststrahlenband.

The lasers have been grown by molecular beam epitaxy on n^+-doped substrates. The active zone consists of 60 periods, each of them containing four quantum wells of the laser transition superlattice plus five injector wells. The Al content of the barriers of $x = 45\%$ for sample A yields the maximum Γ-Γ band offset of 390 meV without introducing indirect barrier states. For sample B, where carrier leakage into the continuum plays a minor role, we considered $x = 35\%$ to be appropriate in order to avoid ultra-thin barriers. The standard waveguide of sample A is a sandwich composed of the active zone embedded in two lightly doped GaAs spacer layers between two n^+-doped confinement layers, see Fig. 1(a) for details. We calculate a waveguide loss coefficient of $\alpha_w = 26$ cm^{-1} and a confinement factor of $\Gamma = 58\%$. The calculated values are for the surface plasmon waveguide of sample B are $\alpha_w = 86$ cm^{-1} and $\Gamma = 80\%$. Notice that the surface plasmon waveguide of sample B is still 22% thinner than the standard waveguide of the shorter wavelength sample A.

The 50 µm wide laser ridges of sample A and B are defined by reactive ion etching. An insulation layer is deposited on the entire surface and later etched away on top of the ridge. After that, a TiAu contact metallization is sputtered onto the top of the structure and onto the backside of the substrate. In case of sample B, a wide window on top of the ridges is left open for subsequent evaporative deposition of the Au plasmon carrying layer. The samples were cleaved to produce Fabry-Pérot resonators of lengths ($L_A = 1330$ µm, $L_B = 1005$ µm).

As illustrated in Fig. 2, lasing occurs on multiple longitudinal modes. The light versus current density characteristics of sample A, displayed in Fig. 3(a), reveal the high performance of this laser: A low threshold current density of $j_{th} = 2.2$ kA/cm^2 and the broad operation current range up to ~4×j_{th} at cryogenic temperatures and a functionality up to a temperature of 220 K. Sample B is characterized by an approximately 5 times higher threshold current density of $j_{th} = 10.2$ kA/cm^2. Consequently the maximal current density is only about ~1.5×j_{th}, and the temperature range is limited to 100 K.

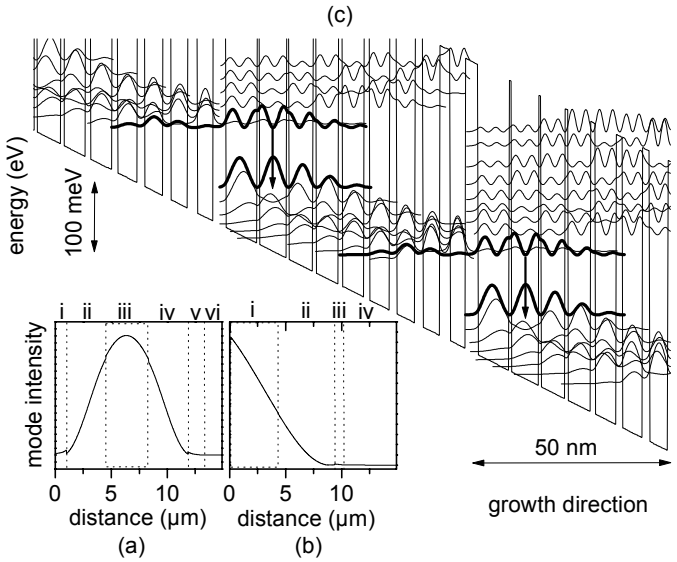

Fig. 1: The calculated optical mode profile (a) for the n^+-confinement waveguide of sample A. The distance is measured from the metal semiconductor interface. The thicknesses [μm] and doping levels [cm^{-3}] of the waveguide layers are: n^+-layer *i* 1.0, 2×10^{18}; spacer *ii* 3.5, 2×10^{16}, active zone *iii* 3.84, 6.5×10^{16}, spacer *iv* 3.5, 2×10^{16}, n^+-layer *v* 0.1, 2×10^{18}, substrate *vi* ~200, ~2×10^{18}. The optical mode profile (b) for the surface plasmon waveguide of sample B with the layers: active zone *i* 4.23, 5.8×10^{16}, spacer *ii* 5.0, 2×10^{16}, n^+-layer *iii* 0.1, 2×10^{18}, substrate *iv* ~200, ~2×10^{18}. The conduction band structure (c) of three periods of sample A at an electric field of 27 kV/cm. The moduli squared of the wavefunction are displayed at their corresponding eigenenergies. The layer thicknesses [nm] of one period, beginning with the injection barrier from left to right, are: **3.2**, 7.8, **0.65**, 6.8, **0.65**, 6.0, **0.8**, 5.5, **1.2**, 5.3, **1.5**, 5.0, **1.8**, 4.6, **2.0**, 4.2, **2.5**, 3.9. $Al_{0.45}Ga_{0.55}As$ barrier thicknesses are typed bold face, GaAs quantum wells normal. The wells corresponding to the underlined thicknesses are Si-doped to $n = 2.3\times10^{17}$ cm^{-3}. The band structure of sample B (not shown) is very similar. The layer thicknesses [nm] are: **3.0**, 9.4, **0.5**, 8.3, **0.55**, 6.8, **1.3**, 5.8, **1.4**, 5.6, **1.5**, 5.4, **1.7**, 5.1, **2.0**, 4.8, **2.3**, 4.5. The barriers are $Al_{0.35}Ga_{0.65}As$ (bold), the wells GaAs. Underlined wells are doped to $n = 2.1\times10^{17}$ cm^{-3}.

The higher threshold current density of sample B originates mainly from two causes to be discussed in the following: 1. the shorter lifetime of carriers in the initial subband of the laser transition, limited by longitudinal optical (LO) phonon emission, and 2. the increased waveguide loss from free carrier and multiphonon absorption. We estimate the threshold current density. The calculation reveals 0.7 kA/cm^2 (A) and 2.9 kA/cm^2 (B) and it underestimates the threshold current densities for both samples by a factor of about three. Even though the calculation cannot account for the absolute values of j_{th}, it can successfully explain the difference between sample A and B. The relaxation time of the initial subband τ_i and the waveguide losses α_w deviate essentially. These are the parameters in which the proximity to the reststrahlenband of 23 μm manifests itself most clearly.

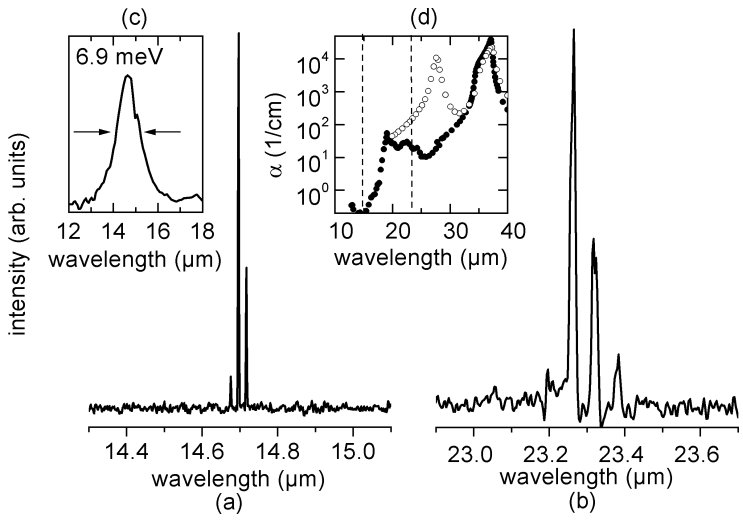

Fig. 2: Laser spectra at a temperature of 5 K (a) of sample A at a current density of 5.1 kA/cm^2 and (b) of sample B at a current density of 11.9 kA/cm^2. The spectra were recorded with a Fourier-transform spectrometer at a resolution of 0.125 cm^{-1} and a liquid N_2-cooled HgCdTe detector. The lasers were operated with 100 ns long pulses at 5 kHz repetition rate. (c) The spontaneous emission spectrum of sample A was measured with the same set up with 2 μm pulses at 50 kHz. (d) The intrinsic absorption coefficient α of undoped bulk GaAs (full symbols) and $Al_{0.14}Ga_{0.86}As$ (open symbols). The emission wavelengths of the two samples are marked with dashed lines.

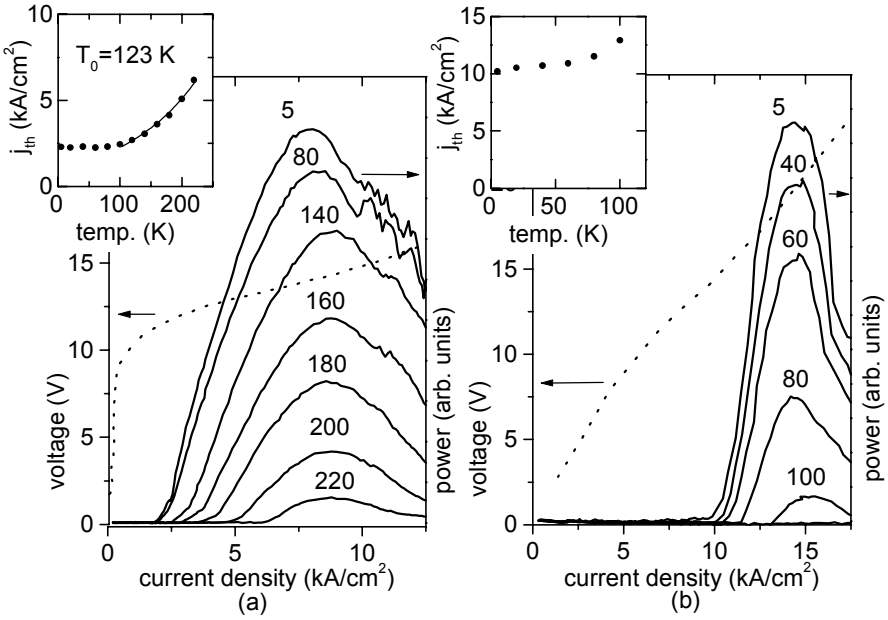

Fig. 3: Light output power (right axis) and voltage (left axis) vs. current density (a) of sample A and (b) of sample B for various temperatures given next to the curves in Kelvin. Pulse conditions and detection technique were the same as for the spectral measurements. The insets show the derived threshold current densities j_{th} vs. the heat sink temperature.